Global Aeroelastic Stability Analysis of a NACA0012 Airfoil in Transitional Reynolds Regime

Diogo Sabino, Olivier Marquet, David Fabre, Vincent Mons

Online Symposium on Aeroelasticity, Fluid-Structure Interaction, and Vibrations
14–15 October 2021
https://www.aeroelasticity2021.com

Global Aeroelastic Stability Analysis of a NACA0012 Airfoil in Transitional Reynolds Regime

Diogo Sabino[1,2], Olivier Marquet[1], David Fabre[2], and Vincent Mons[1]

[1] ONERA-DAAA, 8 rue des Vertugadins, 92190 Meudon, France
E-mail: diogo.ferreira_sabino@onera.fr
[2] Institut de Mécanique des Fluides de Toulouse (IMFT), Université de Toulouse, CNRS, Toulouse, France

Abstract

The onset of pitch-oscillations of a NACA0012 airfoil mounted on a torsion-spring is investigated by the means of a global fluid–structure linear stability analysis (LSA). Experimental studies from literature have shown this configuration undergoing on a flutter behaviour for a close range of Reynolds. This phenomenon is attributed to the laminar character of the boundary layer on the airfoil surface and to its detachment, transition and subsequent reattachment. In this regard, we carried out a global fluid–structure LSA of a mean flow field, issued from a time and spanwise averaged Direct Numerical Simulation, at different incidences, α, for $Re = 50\,000$. The LSA at $\alpha = 0\,^\circ$ predicts a static divergence behaviour of the airfoil from its equilibrium position, whereas the LSA at different incidences predicts the stabilisation of the static mode, associated to the existence of a laminar separation bubble over the upper surface of the airfoil.

Keywords: linear stability analysis, transitional Reynolds regime, laminar separation flutter

1 Introduction

The linear stability of fluid-solid systems is a classic subject on the aeroelasticity community [1]. The primordial aim was to delimit the flight envelope of military and commercial aircraft cruise flights, whose Reynolds number often exceeds a million and where the boundary layer remains turbulent and attached to the airfoil for a relatively hight range of angles of attack. However, as the Reynolds number decreases, the transition location moves downstream, originating a laminar boundary layer over a considerable portion of the wing. For a low-to-moderate Reynolds number range, $10^4 \leq Re \leq 10^6$, the flow regime is characterised by the coexistence of laminar, transition and turbulent regions, where laminar boundary layer region can lead to complex viscous phenomena, such as laminar boundary layer separation, with a possible transition and reattachment.

In this Reynolds regime, Poirel *et al.* [2] carried out a wind tunnel experimental investigation of a NACA0012 airfoil mounted on a torsional spring system, demonstrating the existence of a self-sustained limit cycle oscillation (LCO) within the Reynolds number range of $45 \times 10^3 \leq Re \leq 130 \times 10^3$. This limit cycle was characterised by a Strouhal frequency around $St = 0.06$ and an oscillation amplitude of $\alpha_{max} \approx 5.5°$, around the equilibrium position at $\alpha = 0°$. The authors suggested that the loss of stability of the airfoil at $\alpha = 0°$ and, consequently, the dynamics of the pitch oscillations, were governed by the laminar separation of the boundary layer, either due to the trailing edge separation or to the presence of the laminar separation bubble (LSB). The phenomenon was numerically reproduced by [3] and others, using a time-marching coupled aeroelastic simulation, where it was confirmed that the laminar separation near the trailing edge plays a critical role in initiating and sustaining the pitch oscillations. For this reason, the phenomenon was labelled as *Laminar Separation Flutter* (LSF).

Regarding the global linear stability analysis (LSA), the aim is to evaluate the linear stability character of the dynamical system considered. In the case of coupled fluid–structure systems, several configurations have been studied in the past years [4, 5]. Concerning the LSF, Negi [6] performed a fluid-structure LSA over a NACA0012 airfoil at $Re = 50\,000$ and $\alpha = 0°$ around a mean flow issued from a spanwise and time-averaged time-marching simulation. They found an unstable static mode, responsible for the departure of the structure from its equilibrium position, and further associate the subsequent non-linear oscillation to a sub-critical mode, which would be non-linearly excited.

In this work, we propose to give an insight on the linear behaviour of the mean flow field at $Re = 50\,000$ by the means of a global fluid–structure linear stability analysis for different incidences. In a first time, the analysis is carried out at $\alpha = 0\,^\circ$. This analysis is then followed by a discussion on the mean flow topology as the angle of attack increases, and in a second time, we analyse the cases for $\alpha > 0°$.

2 Mathematical and Numerical Formulations

2.1 Fluid and Solid Models

The dynamics of an incompressible flow field is governed by the Navier–Stokes equations, that can be posed, with respect to a non-inertial frame of reference, as

$$\forall \boldsymbol{X} \in \Omega_f \subset \mathbb{R}^3\,,\, t>0 : \begin{cases} \dfrac{\partial \boldsymbol{U}}{\partial t} + \boldsymbol{\Omega}\times\boldsymbol{U} + \left([\boldsymbol{U}-\boldsymbol{u}_w]\cdot\boldsymbol{\nabla}\right)\boldsymbol{U} + \boldsymbol{\nabla}p - \dfrac{1}{Re}\boldsymbol{\nabla}\cdot\left(\boldsymbol{\nabla}\boldsymbol{U} + (\boldsymbol{\nabla}\boldsymbol{U})^T\right) = \boldsymbol{0}\,, & \text{(1a)} \\ \boldsymbol{\nabla}\cdot\boldsymbol{U} = 0\,, & \text{(1b)} \end{cases}$$

with Ω_f the fluid domain, $\boldsymbol{U}(\boldsymbol{X},\,t) = [U,\,V,\,W]^T$ the absolute fluid velocity field, $p(\boldsymbol{X},\,t)$ the fluid pressure and $\boldsymbol{u}_w$ the airfoil velocity, defined as

$$\boldsymbol{u}_w = \boldsymbol{\Omega}\times(\boldsymbol{X}-\boldsymbol{X}_{EC}) + \dot{\boldsymbol{X}}_{EC} \quad \text{with} \quad \dot{\boldsymbol{X}}_{EC} = U^\infty[-\cos(\theta),\,\sin(\theta),\,0]^T\,. \tag{2}$$

The Reynolds number is defined as $Re = cU^\infty/\nu$, with c the airfoil chord, U^∞ its the translation velocity on the absolute frame and ν the kinematic viscosity. The airfoil is considered as a rigid body, allowed to rotate around its elastic centre, $\boldsymbol{X}_{EC}$, fixed at $0.186c$. The pitching motion is characterised by the instantaneous angular displacement, $\theta(t)$, and by the angular velocity, $\Omega(t)$, both considered positive for a nose-down displacement. $\Omega(t)$ represents the $\boldsymbol{e}_z$-component of the vectorial angular velocity $\boldsymbol{\Omega} = \Omega\,\boldsymbol{e}_z$. Additionally, the angle of attack is defined simply as $\alpha = -\theta$. We consider homogeneous Dirichlet conditions on the inlet and lateral domain boundaries for the velocity field and a natural Neumann condition at the outlet, imposing a stress-free condition. The fluid state vector can be posed as $\boldsymbol{q}_f = [\boldsymbol{U},\,p]^T$.
The Direct Numerical Simulations (DNS) were performed for a fixed airfoil configuration, hence having $\Omega = 0$ and θ fixed on time. The motion of the airfoil is considered for the linear stability analysis formulation, with a temporal evolution defined as

$$I_s(\boldsymbol{X}_{EC})\frac{\mathrm{d}\Omega}{\mathrm{d}t} + D_s\Omega + K_s\theta = m_z\big(\boldsymbol{q}_f,\,\boldsymbol{X}_{EC}\big)\,, \quad \text{with} \quad \frac{\mathrm{d}\theta}{\mathrm{d}t} - \Omega = 0 \tag{3}$$

where I_s is the non-dimensional moment of inertia around the elastic centre position, D_s the non-dimensional structural damping, K_s the non-dimensional structural stiffness and m_z the $\boldsymbol{e}_z$-component of the aerodynamic moment, $\boldsymbol{m} = m_z\boldsymbol{e}_z$, measured around the elastic centre. The corresponding dimensional structure parameters are noted I_s^{dim}, D_s^{dim} and K_s^{dim}.

2.2 Linearised Equations

The linear stability of the airfoil structure is determined by investigating the nature of small amplitude perturbations of a steady state field. In that sense, the the fluid-solid state variable, $\boldsymbol{q}$, is decomposed as the sum of a steady solution $\bar{\boldsymbol{q}} = \left[\bar{\boldsymbol{q}}_f,\,\bar{\theta},\,\overline{\Omega}\right]^T$ and unsteady infinitesimal perturbation $\epsilon\boldsymbol{q}'$ as

$$\boldsymbol{q}(\boldsymbol{X},\,t) = \bar{\boldsymbol{q}}(\boldsymbol{X}) + \epsilon\boldsymbol{q}'(\boldsymbol{X},\,t)\,, \tag{4}$$

where $\epsilon \ll 1$. As the steady solution is independent of time, its angular velocity is equal to zero, $\overline{\Omega} \equiv 0$, unlike the angle of incidence $\bar{\theta} \neq 0$, which can represent the airfoil at a given equilibrium position. The infinitesimal perturbation can be further decomposed into the form of global modes, *i.e.*,

$$\boldsymbol{q}'(\boldsymbol{X},\,t) = \frac{\hat{\boldsymbol{q}}(\boldsymbol{X})\,\mathrm{e}^{\sigma t} + \text{c.c.}}{2}\,, \tag{5}$$

where c.c. is a short hand for complex conjugate, $\hat{\boldsymbol{q}}(\boldsymbol{X})$ is a complex eigenmode with an eigenvalue $\sigma = \lambda + \mathrm{i}\omega$. The eigenmode describes the spatial distribution of the perturbation, whereas the eigenvalue accounts for amplification rate, λ, and frequency characteristics, ω, for that eigenmode. The sign of the amplification rate indicates if the corresponding eigenmode decays (negative sign) or grows (positive sign) exponentially in time, dictating if the steady state is linearly stable or unstable to the eigenmode perturbation. The complex moment of the eigenmode is defined as $\hat{m}_z = \boldsymbol{m}^T\hat{\boldsymbol{q}}_f$.
The steady state is here represented by the mean flow field, issued from the time and spanwise averaged DNS, at different incidences, for $Re = 50\,000$. As the mean flow is averaged in the spanwise direction, the LSA computations are made in a two-dimensional space, having $\hat{\boldsymbol{q}} = \left[\hat{U},\,\hat{V},\,\hat{p}\right]^T$.

Injecting the decomposition 4 into the equations 1 and 3, one obtains, at order ϵ, an eigenvalue problem, that can be put in the form $\sigma \mathsf{M}\hat{\boldsymbol{q}} = \mathsf{L}\hat{\boldsymbol{q}}$:

$$\sigma \begin{bmatrix} \mathsf{M}_f & \mathbf{0} & \mathbf{0} \\ \mathbf{0} & 1 & 0 \\ \mathbf{0} & 0 & I_s \end{bmatrix} \begin{bmatrix} \hat{\boldsymbol{q}}_f \\ \hat{\theta} \\ \hat{\Omega} \end{bmatrix} = \begin{bmatrix} \mathsf{L}_f & \boldsymbol{v}_\theta & \boldsymbol{v}_\Omega \\ \mathbf{0} & 0 & 1 \\ \boldsymbol{m}^T & -K_s & -D_s \end{bmatrix} \begin{bmatrix} \hat{\boldsymbol{q}}_f \\ \hat{\theta} \\ \hat{\Omega} \end{bmatrix}, \tag{6}$$

where M_f is the fluid mass operator, L_f the fluid Jacobian operator, and $\boldsymbol{v}_\theta$, $\boldsymbol{v}_\Omega$ the vector components of the solid motion. $\boldsymbol{v}_\theta$ represents an unitary linear displacement of the airfoil structure, whereas $\boldsymbol{v}_\Omega$ represents an unitary linear angular velocity.

2.3 Numerical Formulation

The spatial discretisation is based on a finite element method. The unknown velocity and pressure fields were discretised using the classical Taylor–Hood basis in order to satisfy the Ladyzhenskaya–Babuška–Brezzi (known as LBB) condition (see, for instance, [7]). All the discrete matrices resulting from the projection of the variational formulations onto the basis of finite elements were built with the *FreeFem++* software [8], and the linear systems solved *via* a parallel implementation using SLEPc/PETSc software [9, 10]. The resolution of the shift-and-invert system passed through an Arnoldi iterative algorithm [11].

3 Results

3.1 Fluid Stability Analysis at $Re = 50\,000$, $\alpha = 0\,^\circ$

We start the analysis by a purely fluid eigenproblem, at $Re = 50\,000$, where the airfoil is fixed at $\alpha = 0°$. The eigenvalue results are presented in the one-sided spectrum in figure 1a, with the growth rate on the horizontal axis and the eigenmode frequency on the vertical axis. A zoom at the origin is plotted in figure 1b. The unstable zone, in grey, corresponds to a positive amplification rate.

The spectrum is characterised by a cloud of stable modes and a single unstable eigenmode, vibrating at a frequency of $\omega = 29.73$. This frequency corresponds to the frequency of the vortex-shedding that can be found on the unsteady airfoil wake. Although this mode is expected to be marginally stable, as in the case of the unsteady vortex shedding on a cylinder wake at supercritical Reynolds regimes [12], the discrepancy can be associated to the high convective character of the perturbation. This fact is in accordance with the conclusions of [2], when they found no correlation between the pitch response frequencies and the vortex–shedding frequency and in accordance with [6], where the projection of the solid variables onto the fluid variables was concluded to be close to zero for all the high frequency eigenmodes.

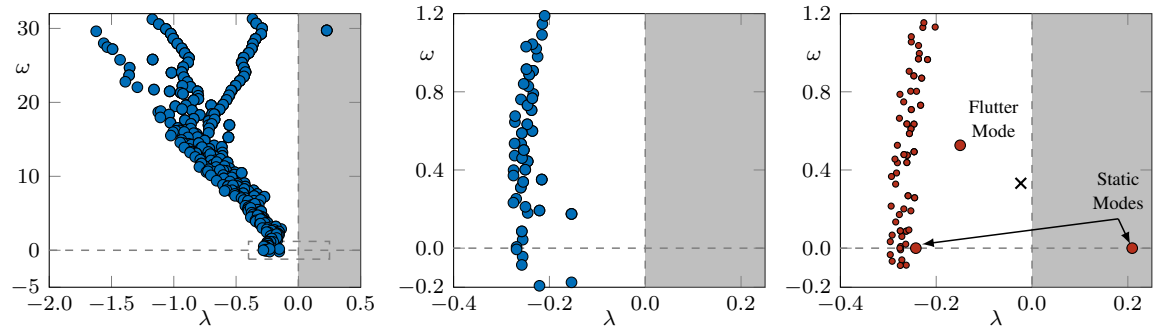

(a) **(b)** **(c)**

Figure 1 – *On the left, the fluid spectrum showing a unstable eigenvalue, with a frequency correspondent to the vortex-shedding frequency. On the centre, a close-up of the same spectrum near the origin. On the right, a fluid–structure spectrum near the origin, highlighting the static and flutter modes, along with the eigenvalue of the structure equation in vacuum, represented by the black cross.*

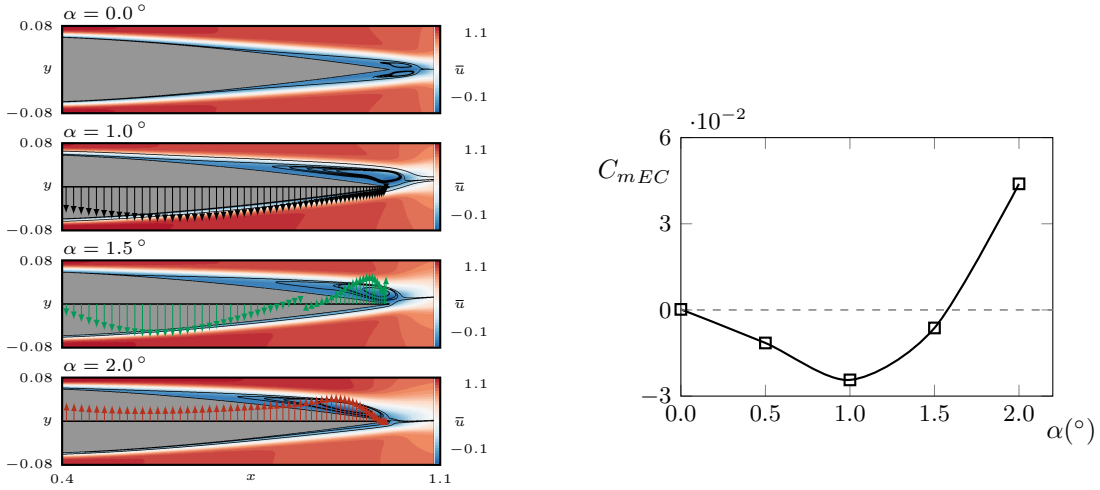

Figure 2 – *At left, the rear airfoil mean flow topology, illustrated by the streamwise velocity component. The resultant forces from the aerodynamics loads applied to the lower and upper surfaces, that contribute to the moment around $\boldsymbol{X}_{EC}$, for each section along the chord, are represented by the vertical arrows. At right, the evolution of the moment coefficient of the mean flow with the angle of attack, showing a first range of incidences where the moment is negative.*

3.2 FSI Stability Analysis at $Re = 50\,000$, $\alpha = 0\,^\circ$

The FSI stability analysis was carried out for the same dimensional parameters as the ones reported in [2] and subsequently used by [6], *i.e.*, $I_s^{dim} = 0.00135\mathrm{kg\,m^2}$, $D_s^{dim} = 0.002\mathrm{N\,m\,s}$ and $K_s^{dim} = 0.15\mathrm{N\,m/rad}$. Figure 1c shows the one-sided spectra of the FSI linear stability analysis. Differently from the hydrodynamic case, the FSI eigenproblem reveals the emergence of two pairs of eigenvalues, associated to the structure. The first pair is located along the real axis, presenting no associated frequency. The unstable eigenmode has a growth rate of $\lambda = 0.2091$, whereas the other eigenvalue is stable and located in the vicinity of the fluid modes. The second pair is located at the a growth rate of $\lambda = -0.1500$ and with a frequency of $\omega = \pm 0.5264$. The eigenmode presenting a divergent character will be labelled *Static Mode*, whereas the low frequency eigenmode, possibly at the origin of the nonlinear flutter oscillations, will be labelled *Flutter Mode*. The flutter mode of the fully coupled fluid–structure problem can be compared with the eigenvalues of the structure equation. The real and imaginary part of these eigenvalues can be computed analytically and read

$$\sigma_s^2 I_s + \sigma_s D_s + K_s = 0 \Rightarrow \lambda_s = -\frac{D_s}{2I_s} \quad \omega_s = \pm\sqrt{\frac{K_s}{I_s} - \lambda_s^2}\,. \tag{7}$$

From this result, one can infer that a structure without damping will be marginally stable, resonating at the natural frequency of $\omega_s = \sqrt{(K_s/I_s)}$. Any positive value of the damping coefficient results into a negative growth rate, damping any structure oscillation, which returns to a stable equilibrium position. For the current parameters, the natural structure eigenvalues are $\sigma_s = -0.0234 \pm 0.3320\mathrm{i}$. The positive frequency eigenvalue can be visualised in the one-sided spectrum of figure 1c and compared to the FSI flutter eigenvalue. The coupled fluid–structure problem gives a more stable mode, suggesting that, for this incidence, the fluid has a stabilising effect on the structure equation.

3.3 FSI Stability Analysis at $Re = 50\,000$, $\alpha > 0\,^\circ$

The DNS computations were further carried out at the incidences from $\alpha = 0.5\,^\circ$ to $\alpha = 2.0\,^\circ$, in order to access to the time and spanwise averaged mean flow field at angles of attack higher than $0\,^\circ$. The streamwise component of the velocity field of the mean flow for four angles of attack is present in the figure 2, at left. The upper figure corresponds to the case at $\alpha = 0\,^\circ$. As illustrated by the streamlines, the flow field has a separation point at $x/c = 0.7$. This separated flow gives rise to a long recirculation bubble that is present in the rear of airfoil, in both lower and upper surfaces. As the angle of attack increases, the separation point on the upper surface of the airfoil moves upstream, while the one on the lower surface moves downstream, the former

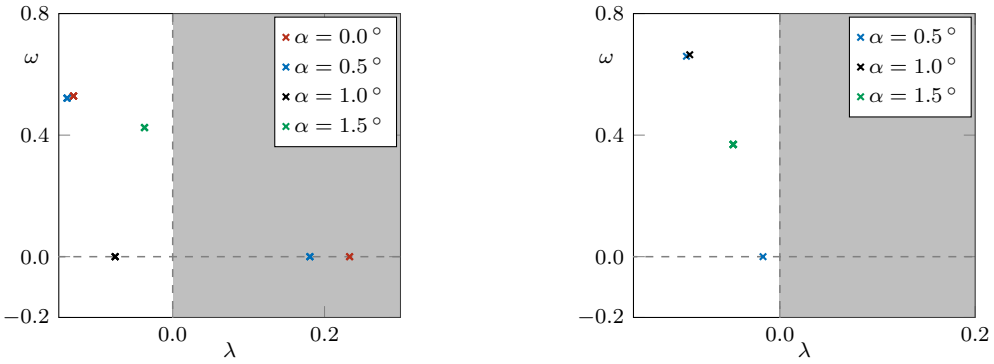

(a) **(b)**

Figure 3 – *At left, the spectrum close to the origin of the FSI LSA analyses, for a fixed* $K_s^{dim} = 0.15\mathrm{N\,m/rad}$*, when varying the angle of attack. At right, the* K_s^{dim} *is varying, such that the equilibrium requirement is met.*

reaching the value of $x/c = 0.46$ for the case at $\alpha = 2\,^\circ$. At this angle, we observe a reattachment of the upper surface separated flow to the rear of the airfoil, giving rise to a recirculation bubble, refereed to as a laminar separation bubble.

The aerodynamic loads acting on each x section along the chord are superposed to the velocity field. Each of these infinitesimal forces contributes to the total moment coefficient evaluated around the elastic centre, X_{EC}, whose evolution, with α, is present in figure 2, at right.

As depicted by the black arrows in the case $\alpha = 1\,^\circ$, the forces at the rear of the airfoil are pointing downwards, generating an initial negative moment coefficient. As the angle increases, the sense of these forces is reversed, starting from the trailing edge, up to the case $\alpha = 2\,^\circ$, where all contributions have an upward sense, generating a positive moment coefficient.

From a static point of view, the initial negative slope of the C_{mEC}–α curve gives us the information that the airfoil has a tendency to pitch-up, as the angle of attack increases. This observation is coherent with the unstable static mode found from the FSI linear stability analysis at $\alpha = 0\,^\circ$. As the angle of attack increases, a second equilibrium can be found, depending on the structural parameters. This second equilibrium position is given by equation 3, after considering a static perturbation in the form $\theta = \bar{\theta} + \epsilon\hat{\theta}\mathrm{e}^{\lambda t}$:

$$\begin{cases} O(1): \quad K_s\bar{\theta} = m_z(\bar{\theta})\,, & \text{(8a)} \\ O(\epsilon): \quad \lambda^2 I_s\hat{\theta} + \lambda D_s\hat{\theta} + K_s\hat{\theta} = \left.\dfrac{\partial m_z}{\partial\theta}\right|_{\theta=\bar{\theta}}\hat{\theta}\,. & \text{(8b)} \end{cases}$$

Noting that $\alpha = -\theta$, equation 8a gives the equilibrium position α, for a given moment coefficient and structure rigidity. The second equation informs us about the presence of an unstable static mode, depending on the slope of the C_{mEC}–α for the considered $\bar{\alpha}$. Further, if one considers $D_s = 0$, the stability criterion can be formed as:

$$\begin{cases} \text{if } \left.\dfrac{\partial m_z}{\partial\alpha}\right|_{\theta=\bar{\theta}} < -K_s \quad \Rightarrow \text{Unstable Static Mode Present}\,, & \text{(9a)} \\ \text{if } \left.\dfrac{\partial m_z}{\partial\alpha}\right|_{\theta=\bar{\theta}} > -K_s \quad \text{No Unstable Static Mode Present}\,. & \text{(9b)} \end{cases}$$

The validity of the above stability criterion is first verified without respecting the equilibrium position. For that, an FSI stability analysis is carried out for the different angles with the rigidity parameters $I_s^{dim} = 0.00135\mathrm{kg\,m^2}$, $D_s^{dim} = 0$ and $K_s^{dim} = 0.15\mathrm{N\,m/rad}$, with the correspondent spectrum present in figure 3a. The results confirm the stability criterion of equation 9, *i.e.*, for the cases $\alpha = 0\,^\circ$ and $0.5\,^\circ$, the slope of the C_{mEC}–α is lower than the rigidity of the airfoil, giving a static unstable eigenmode. On the other hand, for the cases of $\alpha = 1\,^\circ$ and $1.5\,^\circ$, the slope of the C_{mEC}–α is higher than the rigidity of the airfoil, resulting in a stable static mode. We note that, although stable, the flutter mode for the latter case has a higher growth rate, being least stable than the lower angle cases.

The same reasoning can be applied by respecting the equilibrium position on equation 8a. For that, and since the values of C_{mEC} and α are fixed by the DNS, the value of K_s must be adjusted in order to respect the equilibrium. The results are present in figure 3b, for $D_s = 0$. For the case $\alpha = 0.5\,^\circ$, the mode is expected to be marginally unstable, as the slope of C_{mEC}–α matches exactly the slope rigidity. However, the eigenmode is found to be in the stable side of the spectrum. For the higher cases $\alpha = 1.0\,^\circ$ and $\alpha = 1.5\,^\circ$, the static mode becomes stable, as, again, the slope of the C_{mEC}–α is higher than the rigidity of the airfoil. These stable static eigenvalues are not represented in the spectrum as they are mixed with the remaining stable spurious modes. In case at $\alpha = 1.5\,^\circ$, the flutter mode is also found to have moved towards the unstable region, although remaining stable. The change in the frequency of the flutter mode is associated to the fact that the considered rigidity of the structure changes, to match the equilibrium position requirement.

3.4 Conclusion

The onset of pitch-oscillations of a NACA0012 airfoil mounted on a torsion-spring was investigated by the means of a global fluid–structure linear stability analysis, around a mean flow field, issued from the time and spanwise averaged DNS, at different incidences, for $Re = 50\,000$. The results at $\alpha = 0\,^\circ$ show the presence of a static unstable mode, associated to the divergent departure of the airfoil from its equilibrium position. These results are confirmed by the presence of a negative slope on the C_{mEC}–α, corroborating the tendency of the airfoil to pitch-up. The LSA computations were then carried out for different incidences, taking into account the second equilibrium position attained by the airfoil. As the angle of attack increases, the static mode has become stable, whereas the flutter mode, although stable, has approached the marginal axis. As a future work, the authors suggest to increase the Reynolds number, as the case studied represent the lower boundary of the laminar oscillation flutter instability found by [2].

References

[1] R. L. Bisplinghoff, H. Ashley, and R. L. Halfman. *Aeroelasticity*. Addison-Wesley Publishing Company, Cambridge, 1st edition edition, 1955.

[2] D. Poirel, Y. Harris, and A. Benaissa. Self-sustained aeroelastic oscillations of a NACA0012 airfoil at low-to-moderate Reynolds numbers. *Journal of Fluids and Structures*, 24(5):700–719, 2008.

[3] D. Poirel, V. Métivier, and G. Dumas. Computational aeroelastic simulations of self-sustained pitch oscillations of a NACA0012 at transitional Reynolds numbers. *Journal of Fluids and Structures*, 27(8): 1262–1277, 2011.

[4] Pauline Assemat, David Fabre, and Jacques Magnaudet. The onset of unsteadiness of two-dimensional bodies falling or rising freely in a viscous fluid: a linear study. *Journal of Fluid Mechanics*, 690:173–202, 2012.

[5] D. Sabino, D. Fabre, J. S. Leontini, and D. Lo Jacono. Vortex-induced vibration prediction via an impedance criterion. *Journal of Fluid Mechanics*, 890:A4, 2020.

[6] P. S. Negi. *Stability and Transition in Pitching Wings*. PhD thesis, Royal Institute of Technology, Stockholm, 2019.

[7] F. Brezzi and M. Fortin. *Mixed and Hybrid Finite Element Methods*. Springer-Verlag, New York, 1st edition edition, 1991.

[8] F. Hecht. New development in freefem++. *Journal of Numerical Mathematics*, 20(3-4):251–265, 2012.

[9] Vicente Hernandez, Jose E. Roman, and Vicente Vidal. SLEPc: A scalable and flexible toolkit for the solution of eigenvalue problems. *ACM Trans. Math. Software*, 31(3):351–362, 2005.

[10] Satish Balay et al. PETSc users manual. Technical Report ANL-95/11 - Revision 3.14, Argonne National Laboratory, 2021.

[11] Yousef Saad. *Numerical Methods for Large Eigenvalue Problems*. Society for Industrial and Applied Mathematics, 2nd edition edition, 2011.

[12] D. Sipp and A. Lebedev. Global stability of base and mean flows: a general approach and its applications to cylinder and open cavity flows. *Journal of Fluid Mechanics*, 593:333–358, 2007.